18th Australasian Fluid Mechanics Conference
Launceston, Australia
3-7 December 2012

Estimation of Dynamic Stall on Wind Turbine Blades using an Analytical Model

A. Choudhry[1], M. Arjomandi[2] and R. Kelso[3]
[1, 2 and 3] School of Mechanical Engineering
University of Adelaide, Adelaide, South Australia 5005, Australia

Abstract

Dynamic stall on Horizontal Axis Wind Turbines (HAWT) is caused by the rapid increase in the angle of attack due to sudden changes in wind speed and direction. In order to relate the changes in wind speed and direction with the variations in the blade-section angle of attack, an analytical model is proposed to determine the regions of the blade affected by dynamic stall. The so-called threshold radius has been identified and defined as the percentage of the blade length from the HAWT hub beyond which the probability of dynamic stall occurrence falls to zero. The model has been validated against the NREL Phase VI HAWT that was tested in the NASA Ames 24.4 m by 36.6 m wind tunnel.

Introduction

A major cause of unsteady load on the HAWT is the occurrence of dynamic stall on the turbine blades. Dynamic stall is considered to be the delay of stall resulting in drastic increase in the lift experienced by an airfoil as the static stall angle is suddenly exceeded [3]. It is also characterised by hysteresis loops in the force coefficients as the airfoil goes through the pitching cycle and the formation of a large leading-edge vortex during the later stages of the pitching cycle. As the vortex convects over the airfoil and sheds, the airfoil goes into a state of deep stall. After this the flow is completely separated and reattaches only when the angle of attack is brought down to a sufficiently low value. Dynamic stall in HAWTs can be caused by unsteady inflow, yaw misalignment, tower shadow and rapid increases in wind speeds (wind gusts). All these factors result in the rapid variations in the blade angle of attack. The effects of tower shadow and yaw misalignment have been investigated in detail by wind tunnel experiments [2]. Furthermore, it has been suggested that gusts can also lead to a state of dynamic stall [6]. Since the wind turbine blades experience a large increase in lift, the gust loads on the turbine blade are more severe than the stalled loads [1] and are, in some cases, even capable of breaking the turbine blades [14]. The subsequent deep stall, as the primary dynamic stall vortex is shed, can lead to the vibrations of the blade, which in turn, result in adverse effect on the life of the turbine and therefore increase of the maintenance costs associated with the operation of HAWTs.
The effects of dynamic stall on the HAWT blades are significant, however at present no information on the relationship between the actual wind conditions and the dynamic variations of the blade angle of attack exists. Such information will assist in prediction of the regions of wind turbine blades affected by dynamic stall for a particular site.

In the current article, a theoretical method that uses the ambient wind conditions as inputs to determine the distribution of reduced frequency along the blade length at different azimuth angles is proposed. Using this distribution a predictive model for dynamic stall occurrence along a wind turbine blade is achieved. The NREL Phase VI HAWT, which was tested in the NASA Ames 24.4 m by 36.6 m wind tunnel, is used for the purpose of validation of the model. The method outlined in the article, therefore, serves as a toolbox to determine the regions of a HAWT blade where dynamic stall control is required.

Analytical Model

For the purpose of derivation of the dynamic stall predictive model, consider the schematic of a HAWT shown in Fig. 1, which consists of an upwind view of a three-bladed HAWT, the top view and the cross-section of the blade. Fig. 1 illustrates the relationship between the inflow variables and the angles involved for a HAWT.
From Fig. 1, the normal (V_n) and cross-flow (V_c) components of the velocity can be determined by:

$$V_n = V_W \cos\gamma \tag{1}$$

$$V_c = -V_W \sin\gamma \tag{2}$$

The cross-flow velocity vector can be further resolved into the tangential (V_t) and the spanwise (V_s) components:

$$V_t = r\omega + V_c \cos\psi = r\omega - V_W \sin\gamma \cos\psi \tag{3}$$

$$V_s = -V_W \sin\gamma \sin\psi \tag{4}$$

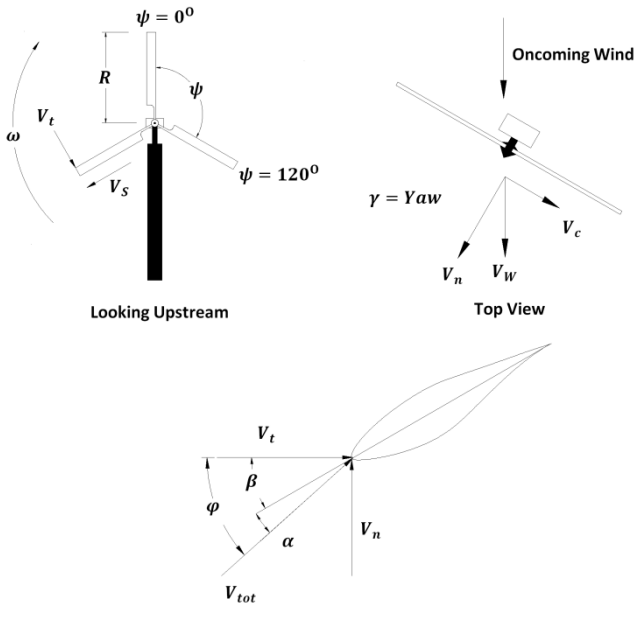

Figure 1. Schematic of a HAWT illustrating the relationship between the inflow variables and the angles involved.

In order to determine the rate of change of angle of attack ($\dot{\alpha}$), angle φ is defined as (Fig. 1):

$$\varphi = \tan^{-1}\frac{V_n}{V_t}$$

Differentiating with respect to time:

$$\frac{d(\varphi)}{dt} = (cos^2\varphi)\left[\frac{V_t\dot{V}_n - V_n\dot{V}_t}{V_t^2}\right]$$

On the other hand since $\alpha + \beta = \varphi$, therefore:

$$\dot{\alpha} + \dot{\beta} = \dot{\varphi}$$

Note that the rate of change of pitch angle ($\dot{\beta}$) is very small as compared to the rate of change of angle of attack. Therefore, ignoring $\dot{\beta}$ results in:

$$\dot{\varphi} = \dot{\alpha} = (cos^2\varphi)\left[\frac{V_t\dot{V}_n - V_n\dot{V}_t}{V_t^2}\right] \quad (5)$$

It can be observed from equation (5) that the rate of change of angle of attack is dependent on the normal and tangential components of the resultant velocity as well as the rate of change of these parameters. Therefore, differentiating equation (1) with respect to time gives:

$$\dot{V}_n = \dot{V}_W \cos\gamma - V_W \sin\gamma \ (\dot{\gamma}) \quad (6)$$

Differentiating equation (3) with respect to time and assuming, for simplicity, a fixed speed rotor ($\dot{\omega} = 0$) yields:

$$\dot{V}_t = -\begin{bmatrix} \dot{V}_W \sin\gamma\cos\psi \\ +V_W\cos\gamma\cos\psi \ (\dot{\gamma}) \\ -V_W\sin\gamma\sin\psi \ (\omega) \end{bmatrix} \quad (7)$$

Note that in equations (6) and (7), $\dot{V}_W$ is the rate of change of ambient wind speed. According to Melbourne [9], the standard deviation in wind speed (or turbulence intensity) can be taken to be the measure of rate of change of wind speed. Similarly $\dot{\gamma}$ is the rate of change of wind direction (or rate of change of yaw angle) and is given by the standard deviation in the wind direction.

Therefore, for a particular site, with some averaged wind conditions, inserting equations (1), (2), (6) and (7) into equation (5) will give the average rate of change of angle of attack at the selected section of the HAWT. Note that the average rate of change of angle of attack is dependent on the ambient wind conditions such as the mean wind speed, mean wind direction, the rate of change of wind speed (turbulence intensity) and the rate of change of wind direction. However, dynamic stall is a complex function of the pitch rate, free-stream velocity and the airfoil geometry [8]. The parameter that incorporates all these factors is termed as the reduced frequency and is given by:

$$k = \pi\frac{\dot{\alpha}c}{V_{tot}} \quad (8)$$

In equation (8), $\dot{\alpha}$ is given by equation (5), c is the chord length of the blade section and V_{tot} is the free-stream velocity experienced at the blade section, given by:

$$V_{tot} = \sqrt{V_n^2 + V_t^2 + V_s^2} \quad (9)$$

Therefore, using the above method, the distribution of reduced frequency along the blade length can be determined based on the ambient wind conditions. Comparison of this distribution with the limiting reduced frequency (the reduced frequency at which the salient features of dynamic stall become evident) can result in the determination of the regions of the turbine blade that are under the influence of dynamic stall. For example, for NACA 0012 airfoil, salient features of dynamic stall surfaced when the limiting reduced frequency was 0.05 [7]. Similarly, it was observed by the authors that for S809 airfoil the limiting reduced frequency was 0.026 [11]. However, beyond these two examples, not much research has been conducted to determine the limiting reduced frequency of airfoils and its dependence on the airfoil geometric properties. Such a study will be extremely useful in the design of airfoils for wind turbines that are inherently resistive to the occurrence of dynamic stall.

From earlier experiments [12], it has been observed that the inboard regions of the turbine blade are highly susceptible to the occurrence of dynamic stall as compared to the outboard regions, due to smaller tangential velocities. Therefore, the frequency and the probability of dynamic stall occurrence reduce from the root towards the tip of the blade, based on the ambient wind conditions and the type of airfoil. Let us define a new parameter known as threshold radius as the percentage of the blade length (or span) from the rotor hub beyond which the probability of dynamic stall occurrence falls to zero based on ambient wind conditions. Therefore, the determination of threshold radius can lead to the calculation of the load distribution on the turbine blade due to dynamic stall and can also assist in possible placement of the control devices for dynamic stall suppression.

It is also important to mention the simplifying assumptions that have been made in the derivation of the model. These include ignoring the effects of axial induction factors, tower wake effects and the skewed wake effects due to yaw. Therefore, the estimations provided in the current article should be considered conservative, since the inclusion of these effects will lead to an increase of threshold radius.

Validation

For the purpose of validation of the model, the NREL Phase VI HAWT was used. The specific HAWT considered here is the one described by Schreck et al. [12] which was tested in the NASA Ames 24.4 m by 36.6 m wind tunnel. The blade of the NREL HAWT is made of S809 airfoil for which the limiting reduced frequency is 0.026. The case study presented here is when the turbine is operating at an rpm of 71.6, mean wind speed of 13 m/s and yaw angle of 40^O. Note that since the wind turbine is operating in the wind tunnel, the rate of change of wind speed and direction ($\dot{V}_W$ and $\dot{\gamma}$ respectively) are zero. The plots of the normal force coefficient at two sections of the turbine blade, under the said operating conditions, are presented in Fig. 2. Note that the trend of the angle of attack at the specific section of the blade can be deciphered from the plots of the normal force coefficients:

$$\frac{dC_n}{d\psi} \propto \frac{d\alpha}{d\psi}$$

Furthermore, the magnitude of the normal force coefficients indicates that the blade is under the influence of dynamic stall during the second half of the rotation cycle ($180^O < \psi < 360^O$) since the maximum normal force coefficient for the S809 airfoil, under steady-state operation, is 0.94 [13]. As it can be seen, for both inboard (0.3R) and outboard regions (0.63R), the normal force coefficients are above 1, indicating dynamic stall for most of the rotation.

The threshold radius was calculated at the selected azimuth angles using the analytical model described in the article based on the aforementioned conditions in the tunnel. Linear variation of the threshold radius was assumed between the selected

azimuth angles. The distribution of the threshold radius with azimuth angle for the NREL HAWT is illustrated in Fig. 3.

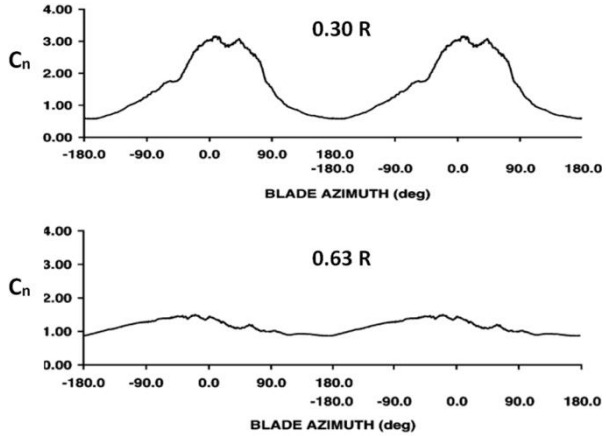

Figure 2. Plots of the normal force coefficient vs. the azimuth angle for two sections along the NREL HAWT blade (0.30 R and 0.63 R). The turbine is operating at an rpm of 71.6, mean wind speed of 13 m/s and a yaw angle of 40^O [12].

It can be observed that the turbine is free of dynamic stall during the first half ($0^O < \psi < 180^O$) of the rotation cycle. This is based on the assumption, as per the original article [12], that pitching in the negative direction (negative reduced frequency) will not cause dynamic stall on the turbine blade This was based on the observation, as shown in Fig. 3, that the normal force coefficients decrease during this part of rotation, indicating a decrease in the angle of attack at both sections of the turbine blade. The assumption was also carried to the analysis performed in the current section for consistency.

However, as stated earlier, during the second half of the rotation cycle ($180^O < \psi < 360^O$) the turbine blade is under the influence of dynamic stall. This is also shown by distribution obtained from the analytical model. The analytical model predicts that approximately between 40-75% of the blade span will be under the influence of dynamic stall during the second half of the rotation cycle. This prediction agrees very well with the results of Schreck et al. [12], who concluded that under the said wind conditions approximately three fourth of the turbine blade (or two third of the aerodynamically active blade) is influenced by dynamic stall.

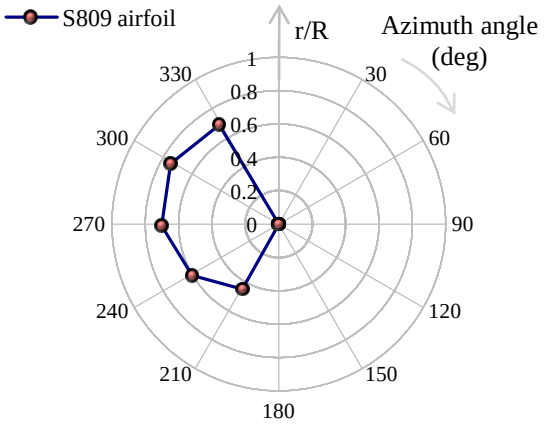

Figure 3. Threshold radius distribution for the NREL Phase VI wind turbine. The turbine is operating at an rpm of 71.6, mean wind speed of 13 m/s and a yaw angle of 40^O.

Therefore, even with the simplifying assumptions, the model proves to be sufficiently accurate to predict the regions of the turbine blade affected by dynamic stall.

Model Inputs

As described earlier, the ambient wind conditions serve as the inputs for the model. Here, the average wind conditions are used to determine the average distribution of threshold radius with azimuth angle. The wind speed and turbulence intensity averaged over one hour of neutral conditions are presented in Fig. 4. Similarly the average wind direction over one hour of neutral conditions is shown in Fig. 5. The original data were collected at the Surface Layer Turbulence and Environmental Science Test (SLTEST) facility in the western salt flats of Utah. Further details regarding the data can be found in [5].

The mean wind speed was fitted using the power law with an exponent of 0.1, as suggested by [4, 15], and the reference height was taken to be 8.71m, as shown in Fig. 4:

$$\frac{V_W(h)}{V_W(8.71\text{ m})} = \left[\frac{h}{8.71}\right]^{0.1} \tag{10}$$

Similarly the turbulence intensity was fitted using the empirical expression developed by Panofsky [10]:

$$I_x = \frac{0.88}{\ln\left(h/h_o\right)} \tag{11}$$

It can be observed that the empirical approximations agree very well with the measured average wind speed and turbulence intensity as presented in Fig. 4.

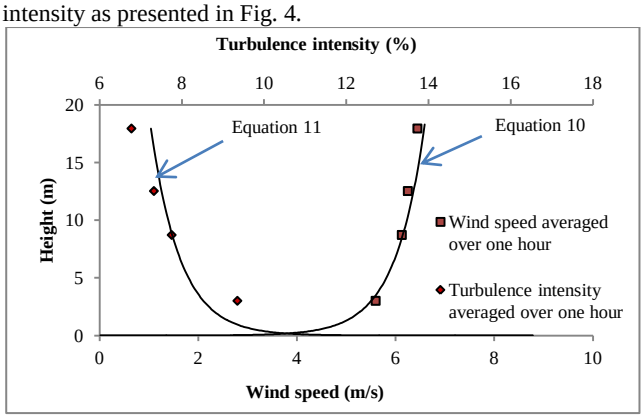

Figure 4. Wind speed and turbulence intensity averaged over one hour. The empirically determined wind speed and turbulence intensity are also shown.

On the other hand, no empirical relations exist to determine the variation of wind direction with height. However, here it can be observed from Fig. 5 that the average wind direction remains approximately constant with height (-11^O). Similarly, standard deviation in wind direction decreases only slightly with height (4^O).

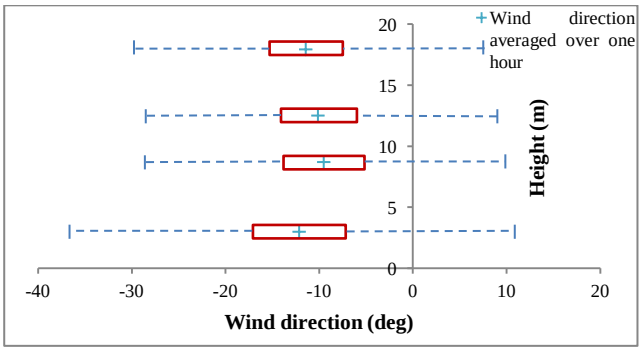

Figure 5. Mean wind direction averaged over one hour. The rectangles represent one standard deviation in the wind direction on either side of the mean. The maximum and the minimum wind direction observed by the anemometers are indicated by the dashed lines.

Case Study

A case study based on the average wind conditions, shown in Fig. 4 and Fig. 5, is presented in this section. Let us consider two theoretical wind turbines that have the same rotor diameter of 15m, tower heights of 10m, constant chord length of 3m along the blade span and operating at an rpm of 30. Let us consider that one of the turbines is composed of the S809 airfoil and the other is composed of the NACA 0012 airfoil. Furthermore, let us assume that both the turbines are experiencing the same wind conditions. In order to illustrate effects of all wind parameters, let us assume that the rotational axis of the turbines is aligned with the principle measurement axis of the anemometers. This implies that the wind direction experienced by the turbines is the same as that shown in Fig. 5 and therefore the turbines are operating at a constant yaw misalignment of -11^{O}. Similarly, the rate of change of yaw angle, given by standard deviation in wind direction, is assumed to be constant with height and equal to 4^{O}/s. The mean wind speed and turbulence intensity are obtained for each height using Fig. 4.

Under these conditions, the average threshold radius distribution for the two turbines is illustrated in Fig. 6. Note that in this case, negative pitching is also considered to be the cause of dynamic stall since for symmetric airfoils negative pitching will generate the similar unsteady response as positive pitching.

It can clearly be observed that due to the larger limiting reduced frequency, NACA 0012 airfoil is inherently more resistive to the occurrence of dynamic stall. This is indicated by the smaller threshold radius at all azimuth angles when compared with the S809 case. Note that approximately 90% of the S809-blade is affected by dynamic stall, whereas only 70% of the NACA 0012-blade is affected under the same wind conditions. From Fig. 6, it can be observed that the effects of yaw misalignment and rate of change of yaw angle are asymterical to the threshold radius. Moreover due to negative yaw angle, the blades are affected more by dynamic stall during the first half of the rotation cycle. Fig. 6 presents the average threhsold radius observed by the turbines. Therefore if the same conditions persist, it is easily deduceable that the turbine with NACA 0012 airfoil has a longer operation life and/or larger intervals between maintenance runs.

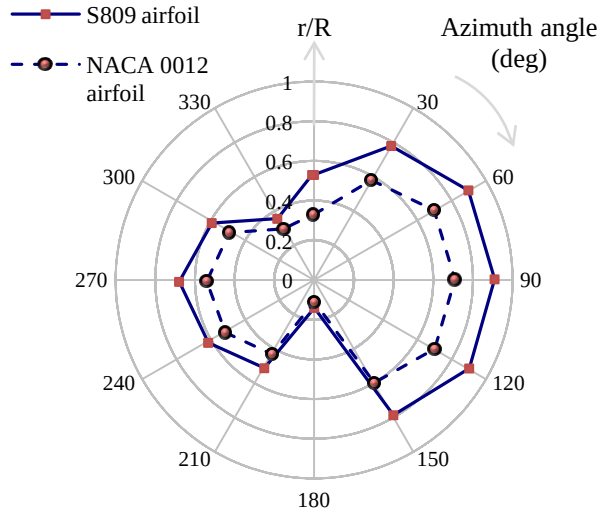

Figure 6. Comparison of the distribution of threhsold radius for two theoretical wind turbines, comprised of two different airfoils, based on the hourly averaged wind conditions presented in Fig. 4 and Fig. 5.

Conclusions

The threshold radius, defined as the percentage of the blade length from the rotor hub beyond which the probability of dynamic stall occurrence falls to zero, has been determined using an analytical model presented in the article. The model was validated against the experiments conducted by NREL for a yawed HAWT and a very good agreement was observed between the theoretical predictions and experimental results. Finally the threshold radius was computed for two theoretical wind turbines using hourly averaged wind conditions. The NACA 0012-blade was observed to be more resistive to the occurrence of dynamic stall, due to larger limiting reduced frequency, as compared to the S809-blade. The case study provides the motivation to conduct research in the design of airfoils that are inherently resistive to dynamic stall. The model presented in this article also can be used to determine the regions of the wind turbine blade affected by dynamic stall based on ambient wind conditions. Hence, the model provides the means for economical situation of the control devices for dynamic stall suppression on wind turbine blades.

References

[1] Burton, T., *Wind Energy: Handbook*, John Wiley & Sons, Ltd, 2001.

[2] Butterfield, C.P., Simms, D., Scott, G. and Hansen, A.C., *Dynamic Stall on Wind Turbine Blades*, National Renewable Energy Lab., Golden, CO (United States), 1993.

[3] Carr, L.W. & Chandrasekhara M., *Compressibility Effects on Dynamic Stal,*. Progress in Aerospace Sciences, 1996. 32(6): p. 523-573.

[4] Holmes, J.D., *Wind Loading of Structures*, Spon Pr., 2001.

[5] Hutchins, N. and I. Marusic, Evidence of very Long Meandering Features in the Logarithmic Region of turbulent Boundary Layers, *Journal of Fluid Mechanics*, 2007. 579: p. 1.

[6] Larsen, J.W., Nielsen S.R.K., and Krenk S., Dynamic Stall Model for Wind Turbine Airfoils, *Journal of Fluids and Structures*, 2007. 23(7): p. 959-982.

[7] McCroskey, W.J., Carr L.W., and McAlister K.W., Dynamic Stall Experiments on Oscillating Airfoils, *AIAA Journal*, 1976. 14(1): p. 57-63.

[8] McCroskey, W.J., McAlister, K.W., Carr, L.W. and Pucci, S.L., *An Experimental Study of Dynamic Stall on Advanced Airfoil Sections. Volume 1: Summary of the Experiment*, NASA Technical Memorandum, 1982 (TM 84245).

[9] Melbourne, W., Criteria for Environmental Wind Conditions, *Journal of Wind Engineering and Industrial Aerodynamics*, 1978. 3(2-3): p. 241-249. 10

[11] Panofsky, H., A survey of current throught on wind properties relevant for diffusion in the lowest 100 m, in *Symp. Atm. Turb. Diffusion*, Sandia Laboratories, Albuquerque, NM, 1967: p. 47-58.

[10] Ramsay, R.R., Hoffmann, M.J., and Gregorek, G.M., *Effects of Grit Roughness and Pitch Oscillations on the S809 Airfoil*, NREL/TP-442-7817, National Renewable Energy Laboratory, Golden, CO. 1995.

[12] Schreck, S.J., Robinson, M.C., Hand, M.M. and Simms, D.A., Blade dynamic stall vortex kinematics for a horizontal axis wind turbine in yawed conditions, *Journal of Solar Energy Engineering*, 2001. 123: p. 272.

[13] Somers, D.M., *Design and experimental results for the S809 airfoil*. 1997, National Renewable Energy Lab., Golden, CO (United States).

[14] Sun, M. & Sheikh, S., Dynamic stall suppression on an oscillating airfoil by steady and unsteady tangential blowing, *Aerospace Science and Technology*, 1999. 3(6): p. 355-366.

[15] Zoumakis, N., The dependence of the power-law exponent on surface roughness and stability in a neutrally and stably stratified surface boundary layer, *Atmosfera*, 2009. 6(1).